



# High-redshift JWST Observations and Primordial Non-Gaussianity

Matteo Biagetti<sup>1,2,3,4</sup> , Gabriele Franciolini<sup>5,6</sup> , and Antonio Riotto<sup>7,8</sup><sup>1</sup> Institute for Fundamental Physics of the Universe, Via Beirut 2, I-34151 Trieste, Italy; [mbiagett@sissa.it](mailto:mbiagett@sissa.it)<sup>2</sup> SISSA—International School for Advanced Studies, Via Bonomea 265, I-34136 Trieste, Italy<sup>3</sup> Istituto Nazionale di Astrofisica, Osservatorio Astronomico di Trieste, via Tiepolo 11, I-34143 Trieste, Italy<sup>4</sup> Istituto Nazionale di Fisica Nucleare, Sezione di Trieste, via Valerio 2, I-34127 Trieste, Italy<sup>5</sup> Dipartimento di Fisica, Sapienza Università di Roma, Piazzale Aldo Moro 5, I-00185, Roma, Italy<sup>6</sup> INFN, Sezione di Roma, Piazzale Aldo Moro 2, I-00185, Roma, Italy<sup>7</sup> Département de Physique Théorique and Centre for Astroparticle Physics (CAP), Université de Genève, 24 quai E. Ansermet, CH-1211 Geneva, Switzerland<sup>8</sup> Gravitational Wave Science Center (GWSC), Université de Genève, CH-1211 Geneva, Switzerland

Received 2022 October 27; revised 2023 January 23; accepted 2023 January 23; published 2023 February 16

## Abstract

Several bright and massive galaxy candidates at high redshifts have been recently observed by the James Webb Space Telescope. Such early massive galaxies seem difficult to reconcile with standard  $\Lambda$  cold dark matter model predictions. We discuss under which circumstances such observed massive galaxy candidates can be explained by introducing primordial non-Gaussianity in the initial conditions of cosmological perturbations.

*Unified Astronomy Thesaurus concepts:* Galaxy dark matter halos (1880); High-redshift galaxy clusters (2007); Primordial galaxies (1293)

## 1. Introduction

The standard cosmological model, based on the idea that the energy budget of the universe is currently dominated by a tiny cosmological constant  $\Lambda$  plus cold dark matter ( $\Lambda$ CDM), predicts that the initial seeds for galaxy formation are halos with relatively low masses of the order of  $10^6 M_\odot$ .

The initial James Webb Space Telescope (JWST) imaging via early release programs, such as Cosmic Evolution Early Release Science (CEERS), early release observations, and early release science (ERS), has recently reported a population of surprisingly massive galaxy candidates at redshifts of  $z \gtrsim 8$  with stellar masses of the order of  $10^9 M_\odot$  (Atek et al. 2023; Finkelstein et al. 2022; Harikane et al. 2022; Naidu et al. 2022; Yan et al. 2022). Even though a spectroscopic follow-up will be necessary to confirm these observations based on photometry only, the early formation of massive galaxies reported by the JWST is hardly reconcilable with the standard  $\Lambda$ CDM expectations, which would require an implausible high star formation efficiency (SFE), even larger than the cosmic baryon mass budget in collapsed structures. It is important to stress though that various uncertainties affect the JWST measurements and might solve the tension with  $\Lambda$ CDM. For example, the calibration of JWST data may cause imprecise redshift determination (see, e.g., Steinhardt et al. 2022; Adams et al. 2023), while the estimation of the stellar masses may be plagued by systematic uncertainties in the initial mass distribution, the effect of a large scatter in the star formation (Mirocha & Furlanetto 2023), the impact of dust attenuation (Ziparo et al. 2022), as well as the inclusion of very bright lines from other sources beyond the stellar continuum (e.g., Endsley et al. 2022). Spectroscopic follow-up and further testing of these astrophysical uncertainties will soon shed more light on the issue.

A useful quantity to assess the viability of the  $\Lambda$ CDM model is the stellar mass density  $\rho_*( > M_*)$  predicted above a given mass scale  $M_*$ . The stellar mass is related to the average baryon mass within each halo through the SFE, which we define as  $\epsilon$ , by the relation

$$M_* = \epsilon (\Omega_b / \Omega_m) M = \epsilon f_b M, \quad (1)$$

with  $M$  being the halo mass and  $f_b = 0.156$  the baryon fraction as measured by Planck (Aghanim et al. 2020). In the following, and in order to be on the conservative side, we will identify the stellar mass with the baryon mass contained within a given halo, which means fixing the SFE to  $\epsilon = 1$ . This conservative choice maximizes the stellar mass predicted by a given scenario.

The comoving cumulative stellar mass density contained within galaxies above a certain stellar mass  $M_*$  reads

$$\rho_*( > M_*, z) = \epsilon f_b \int_{M_*/(\epsilon f_b)}^{\infty} \frac{dn(M, z)}{dM} M dM, \quad (2)$$

where  $n(M)$  is the CDM HMF.

Recently, based on 14 galaxy candidates with masses in the range  $\sim 10^9 - 10^{11} M_\odot$  at  $7 < z < 11$  identified in the JWST CEERS program, Labbe et al. (2022) derived the cumulative stellar mass density at  $z = 8$  and 10 for  $M_* \gtrsim 10^{10} M_\odot$ . They found at  $z \simeq 10$

$$\begin{aligned} \rho_*( > 10^{10} M_\odot) &\simeq 1.3_{-0.6}^{+1.1} \cdot 10^6 M_\odot \text{ Mpc}^{-3}, \\ \rho_*( > 10^{10.5} M_\odot) &\simeq 9_{-6}^{+11} \cdot 10^5 M_\odot \text{ Mpc}^{-3}. \end{aligned} \quad (3)$$

These values are larger than  $\Lambda$ CDM predictions by a factor  $\sim 50$ , even allowing for a maximum efficiency of  $\epsilon = 1$ , or invoking extreme value statistics (Lovell et al. 2023).

While several extensions of the  $\Lambda$ CDM scenario have been already put forward in the recent literature (Gong et al. 2022; Liu & Bromm 2022; Menci et al. 2022), they all appeal to new ingredients in the late-time evolution of the universe. The goal of this paper is to discuss a possible solution which invokes a change in the initial conditions of the cosmological

perturbations giving rise to the DM halos, that is, non-Gaussianity (NG; Bartolo et al. 2004). Indeed, a possible source of NG could be primordial in origin, being specific to a particular mechanism for the generation of cosmological perturbations. It is known that NG in the initial conditions may change the abundance of DM halos, especially in the high mass range of the HMF. As such, primordial NG may provide in principle a boost in forming high mass and bright galaxies. In the following, we characterize the nature of NG, specifying which properties NG has to possess to be in agreement with the JWST data.

The paper is organized as follows. In Section 2 we discuss how one can model the Gaussian and NG HMFs, by also checking their validity with dedicated  $N$ -body simulations. In Section 3 we compare models with various NG signatures to the JWST data, while our conclusions are offered in Section 4.

## 2. Halo Mass Function

### 2.1. Gaussian

We describe the Gaussian differential halo abundance as

$$\frac{dn}{dM} = F(\nu) \frac{\bar{\rho}_M}{M^2} \frac{d \ln \sigma^{-1}}{d \ln M}, \quad (4)$$

where  $\bar{\rho}_M$  is the background average matter density,  $\nu = \delta_c / \sigma(M, z)$  with  $\delta_c = 1.686$  corresponding to the critical linear overdensity for collapse, while  $\sigma(M, z)$  is the variance of the smoothed linear density field. The smoothing scale  $R$  is related to the halo mass through the relation  $R = (3M/4\pi\bar{\rho}_M)^{1/3}$ . Linear density fields evolve with time according to the linear growth factor  $D(z)$ , and we assume a CDM form for the linear power spectrum. The variance of linear density perturbations smoothed on scale  $R$  is therefore computed as

$$\sigma^2 = \langle \delta^2 \rangle = \int \frac{d^3k}{(2\pi)^3} W^2(kR) \mathcal{M}^2(k, z) P_\zeta(k), \quad (5)$$

where  $P_\zeta(k)$  is the linear comoving curvature power spectrum, defined from the curvature field two-point function

$$\langle \zeta(\mathbf{k}_1) \zeta(\mathbf{k}_2) \rangle \equiv (2\pi)^3 \delta_D(\mathbf{k}_1 + \mathbf{k}_2) P_\zeta(k_1). \quad (6)$$

Also, we introduced the Fourier transform of a top-hat spherical window function

$$W(kR) = 3 \left( \frac{\sin(kR)}{(kR)^3} - \frac{\cos(kR)}{(kR)^2} \right), \quad (7)$$

and we defined

$$\mathcal{M}(k, z) = \frac{2}{5} \frac{k^2 T(k) D(z)}{\Omega_M H_0^2} \quad (8)$$

in terms of the linear transfer function  $T(k)$ , the matter abundance  $\Omega_M$ , and the present day Hubble rate  $H_0$ , following the standard conventions in the literature.

### 2.2. NG

The presence of NGs in the initial conditions alters the abundance of DM halos. Several ways of modeling this effect have been proposed in the past (see, e.g., Biagetti 2019 for a recent review, and references therein).

The general approach is based on the Edgeworth expansions of the probability distribution function of the matter density field, or of the level excursion probability of overcoming a threshold for collapse (Matarrese et al. 2000; LoVerde et al. 2008; Desjacques & Seljak 2010). In the limit of a weak-enough NG, the expansion is usually truncated to the leading term, which is generated by the three-point function of the primordial field. As a result, the exponential tail of the mass function (Equation (4)) is modified by a non-vanishing skewness, and one can correct the Gaussian HMF with a multiplicative factor

$$\frac{dn_{\text{NG}}}{dM} = \frac{dn}{dM} \times C_{\text{NG}}(M), \quad (9)$$

which we take to be the one proposed by Desjacques & Seljak (2010):

$$C_{\text{NG}}(M) = \left[ \frac{\hat{\delta}_c^2}{6\Delta} \frac{dS_3}{d \ln \sigma} + \Delta \right] \times \exp \left( \frac{S_3 \hat{\delta}_c^3}{6\sigma^2} \right). \quad (10)$$

Here we introduced  $\hat{\delta}_c = 0.949 \times \delta_c$  and  $\Delta \equiv \sqrt{1 - \hat{\delta}_c S_3/3}$ , and the skewness  $S_3$  can be computed by integrating the matter bispectrum

$$S_3 \equiv \frac{\langle \delta^3 \rangle}{\sigma^4} = \frac{1}{\sigma^4} \int \left( \prod_{i=1}^3 \frac{d^3k_i}{(2\pi)^3} \right) \mathcal{B}(\mathbf{k}_1, \mathbf{k}_2, \mathbf{k}_3), \quad (11)$$

which in turn is sourced by the primordial curvature bispectrum  $B_\zeta$  through

$$\mathcal{B}(\mathbf{k}_1, \mathbf{k}_2, \mathbf{k}_3) = \mathcal{M}(k_1, z) \mathcal{M}(k_2, z) \mathcal{M}(k_3, z) \times B_\zeta(k_1, k_2, k_3). \quad (12)$$

The specific type of NG that sources the change in the halo mass function (HMF) is fully specified by  $B_\zeta$  in a model-dependent way. In this work, we focus on the so-called *local*-type NG, which includes a class of models where local interactions among fields take place on superhorizon scales (see Bartolo et al. 2004 for a review).

For these models, the primordial bispectrum takes the simple, factorizable, form of

$$B_\zeta(k_1, k_2, k_3) = \frac{6}{5} f_{\text{NL}} [P_\zeta(k_2) P_\zeta(k_3) + \text{perm}], \quad (13)$$

where  $f_{\text{NL}}$  parameterizes the amplitude of the bispectrum and  $P_\zeta$  is the primordial curvature power spectrum.<sup>9</sup> While in the most popular version of the local NG  $f_{\text{NL}}$  is scale independent, in our comparison with JWST data we are going to test extensions that allow  $f_{\text{NL}}$  to run with scale. This generalization is well motivated for several models of interactions taking place during inflation (Chen 2005; Khoury & Piazza 2009; Byrnes et al. 2010, 2011; Huang 2010a, 2010b; Riotta & Sloth 2011), and its implications have been thoroughly investigated in cosmic microwave background (CMB)

<sup>9</sup> Assuming a constant  $f_{\text{NL}}$ , one can show by directly integrating Equation (11) that an accurate fit of the skewness as a function of both scale and redshift is given by (see, e.g., Chongchitan & Silk 2010)

$$S_3(M, z) = \frac{1.8 \times 10^{-4} f_{\text{NL}}}{\sigma^{0.838}(M, z) D^{0.162}(z)}, \quad (14)$$

which we adopt in the remainder of this work when dealing with a constant  $f_{\text{NL}}$ . We have checked that the fit is accurate even up to redshifts  $z \simeq 10$ .

observations and for galaxy surveys observing at low redshift (LoVerde et al. 2008; Sefusatti et al. 2009; Becker et al. 2011, 2012; Agullo & Shandera 2012; Giannantonio et al. 2012; Biagetti et al. 2013a, 2013b). The corresponding bispectrum in this scale-dependent model is

$$B(k_1, k_2, k_3) = \frac{6}{5} [f_{\text{NL}}(k_1)P_\zeta(k_2)P_\zeta(k_3) + \text{perm}], \quad (15)$$

where different functional forms for  $f_{\text{NL}}(k)$  that we adopt are specified in the next section.

### 2.3. Testing High-redshift Halo Mass Functions with N-body Simulations

Previous literature has thoroughly compared theoretical predictions of the HMF both for Gaussian (Jenkins et al. 2001; Evrard et al. 2002; Reed et al. 2003, 2007; Warren et al. 2006; Lukic et al. 2007; Cohn & White 2008; Tinker et al. 2008, 2010; Despali et al. 2015) and NG (Matarrese et al. 1991; Moscardini et al. 1991; Park et al. 1991; Gooding et al. 1992; Weinberg & Cole 1992; Borgani et al. 1994; Dalal et al. 2008; Pillepich et al. 2010; Achitouv & Corasaniti 2012; Achitouv et al. 2014; Stahl et al. 2023) initial conditions to simulations. However, most results are at low redshifts,  $z \lesssim 2$ , and none of them include comparisons at higher redshifts including NG initial conditions. Hence, it is important to validate the predictions at the redshifts of relevance for the galaxies observed by JWST that are discussed in this paper.

To perform our analysis, we use a subset of the EOS DATA SET,<sup>10</sup> which includes simulations with Gaussian as well as NG initial conditions. The initial particle displacement is generated at  $z_{\text{in}}=99$  using 2LPTIC (Scoccimarro 1998), and its extended version (Scoccimarro et al. 2012) for local NG initial conditions, using  $f_{\text{NL}}=500$  as the value for the nonlinearity parameter. The linear power spectrum given as an input is computed using CLASS (Blas et al. 2011) and assumes a flat  $\Lambda$ CDM cosmology with  $n_s=0.967$ ,  $\sigma_8=0.85$ ,  $h=0.7$ ,  $\Omega_m=0.3$ , and  $\Omega_b=0.045$ . The public code Gadget2 (Springel 2005) is used to evolve  $512^3$  particles in a cubic box of  $64 \text{ Mpc } h^{-1}$  per side, which allows enough resolution to resolve DM halos down to  $M \sim 10^{10} M_\odot$ . We run 30 different realizations for both the Gaussian and NG initial conditions. We identify halos in each simulation using the code ROCKSTAR (Behroozi et al. 2013), with a lower mass cut off of a minimum of 100 particles, resulting in halos of minimum  $M_{\text{min}} \simeq 2.3 \times 10^{10} M_\odot$ . The algorithm used is Friends-of-Friends with a linking length of  $\lambda=0.28$  at redshifts of  $z=8$  and 10 and it estimates the halo mass with a spherical overdensity (SO) approach, with an overdensity of  $\Delta = 200 \bar{\rho}_M$ .

As already shown in Biagetti et al. (2017) for a similar set of halos at redshifts of  $z=0, 1$ , and 2, the Tinker fit (Tinker et al. 2010) provides good agreement with the HMF measured in the simulations. Hence, in what follows, we adopt the Tinker HMF parameterized as

$$\begin{aligned} F_{\text{Tinker}} &= 0.368 [1 + (\beta\nu)^{-2\phi}] \nu^{2\eta+1} e^{-\gamma\nu^2/2}, \\ \beta &= 0.589(1+z)^{0.2}, \quad \phi = -0.729(1+z)^{-0.08}, \\ \eta &= -0.243(1+z)^{0.27}, \quad \gamma = 0.864(1+z)^{-0.01}, \end{aligned} \quad (16)$$

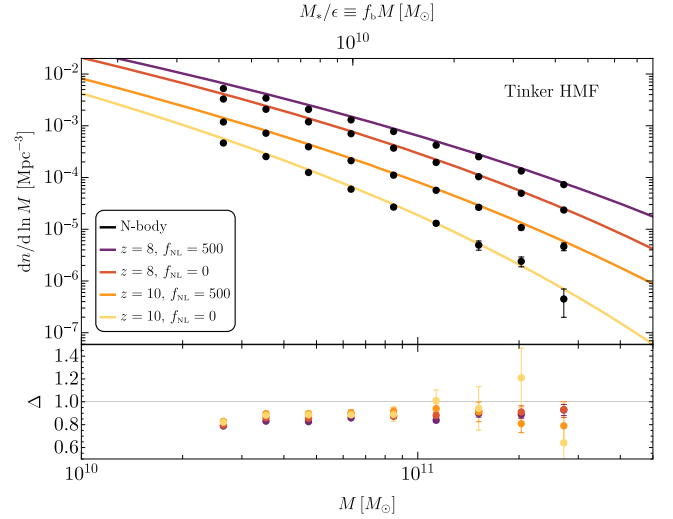


**Figure 1.** Halo mass distribution at redshifts of  $z=8$  and  $z=10$  assuming either Gaussian or NG ( $f_{\text{NL}}=500$ ) curvature perturbations and compared to  $N$ -body simulations (see the main text). The bands around the simulation data points indicate the standard error on the mean. In the bottom panel, we show the ratio between the simulation data points and the Tinker fit  $\Delta \equiv (dn_{\text{sim}}/d \ln M)/(dn_{\text{Tinker}}/d \ln M)$ , adopting the same color code as in the top panel.

where  $\nu$  is computed using the same linear power spectrum provided as input to the simulations.

In Figure 1, we show the HMF at various redshifts in the absence of NGs and assuming NG initial conditions of the local type with  $f_{\text{NL}}=500$ . The model agrees within 20% of the measurements both for the Gaussian and NG initial conditions even at  $z=8$  and 10. These differences are reasonable, given that the Tinker mass function has not been tested at such high redshifts and that the Rockstar halo finder is not a fully SO algorithm. Thus, we are confident that our theoretical predictions for the HMF are realistic within the approximations made.

### 3. The JWST Data and NGs

Based on the results of the previous section, we compute the (comoving) cumulative stellar mass density contained within galaxies above a certain stellar mass  $M_*$  by integrating Equation (2) and including the presence of local NGs. For these computations we use a value of  $\sigma_8=0.815$ , which is closer to the current best-fit model quoted in the latest Planck results (Aghanim et al. 2020). All other cosmological parameters are taken to be the same as the simulated data presented in the previous section.

In Figure 2 we show a comparison between the JWST observations from Labbe et al. (2022) and the heavy halo star density for different values of  $f_{\text{NL}}$  in the case where  $f_{\text{NL}}$  is constant. Large NGs can easily reduce the tension with the observations at a redshift of  $z \approx 10$  but do not help explain the mild evolution between the two redshift bins.

Such large NGs are, however, ruled out by CMB anisotropy data (Akrami et al. 2020) and eBOSS clustering data (Castorina et al. 2019), which constrain local-type NGs to be of order  $|f_{\text{NL}}| \lesssim 10$  and  $|f_{\text{NL}}| \lesssim 26$  at the 95% confidence level, respectively. On the other hand, one should take into account the fact that these constraints are valid at relatively large scales,  $k_{\text{constraints}} \lesssim 0.3 h \text{ Mpc}^{-1}$ , while the relevant scale for these massive galaxies at redshifts of  $z=8$  and 10 is

<sup>10</sup> Information on the EOS suite is available at <https://mbiagetti.gitlab.io/cosmos/nbody/eos/>.

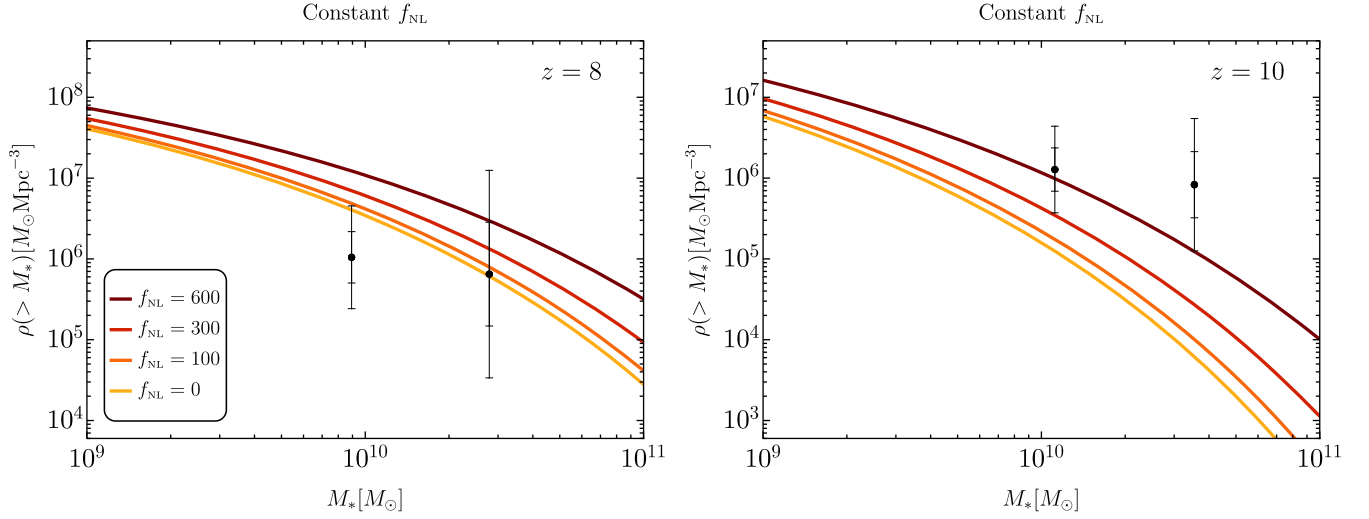


**Figure 2.** Left: co-moving cumulative stellar mass density of galaxies with a stellar mass above  $M_*$  at a redshift of  $z = 10$ . The black bars indicate the  $1\sigma$  and  $2\sigma$  ranges inferred from the JWST observations (Labbe et al. 2022), where the latter is extrapolated assuming a Gaussian distribution. The same convention is used in the following figures. For a comparison of the JWST observations of Labbe et al. (2022) with other data sets, see, for example Lovell et al. (2023). Right: same as the top panel but for  $z = 8$ .

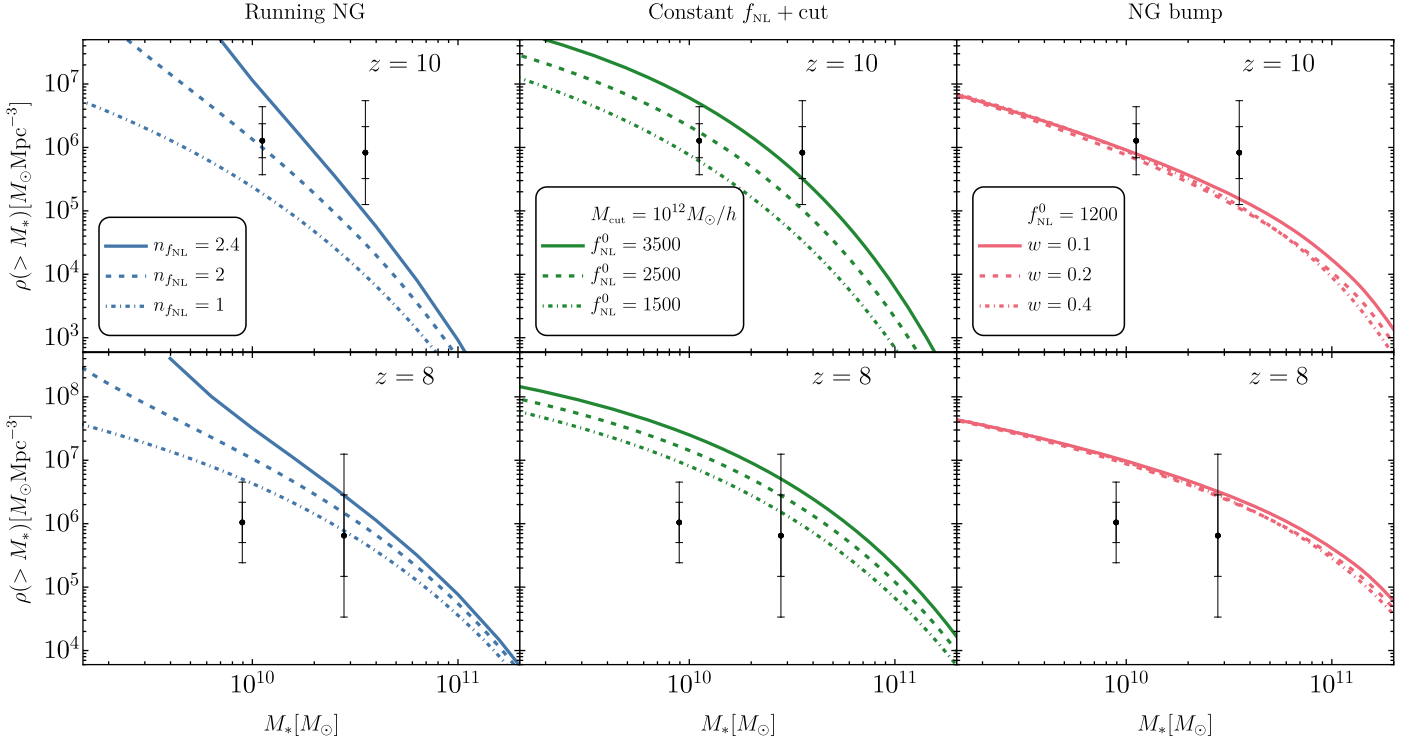


**Figure 3.** Stellar mass density above  $M_*$  as shown in Figure 2 assuming different NG models. We emphasize that we conservatively assume the stellar mass is comparable to the baryon mass contained within a given halo ( $\epsilon \simeq 1$ ). As such, a satisfactory resolution of the tension would require the lines to fall above the data points. Note that the corresponding value of  $f_{\text{NL}}^0$  should depend on  $\epsilon$  if more realistic values ( $\epsilon < 1$ ) are chosen. Left: the running-NG model. Center: constant NG with a sharp cut at the scale corresponding to halo masses  $M_{\text{cut}}$ . In the lower panel, transitions to negligible values of  $S_3$  bring the predictions toward the Gaussian case (as can be seen in the lower panel). Right: NG bump.

$k \sim 1/R \gtrsim 1.5 h \text{ Mpc}^{-1}$ , where we choose  $R$  to be the Lagrangian radius corresponding to halo masses of  $M \sim 10^{11} M_\odot$ , which are considered in our analysis (i.e., stellar masses around  $M_* \sim 10^{10} M_\odot$ ). Around these small scales, Sabti et al. (2021) have put constraints using UV galaxy luminosity functions from the Hubble Space Telescope (HST) of about  $f_{\text{NL}} \lesssim 500$  at the 95% confidence level, but assuming that NGs are switched on already at scales of

$k_{\text{cut}} \sim 0.15 h \text{ Mpc}^{-1}$ . With increasing  $k_{\text{cut}}$ , the constraints loosen considerably (Sabti et al. 2021).

We therefore consider the possibility that the  $f_{\text{NL}}$  parameter runs enough with scale to evade current constraints and simultaneously explain the JWST high-redshift galaxies.

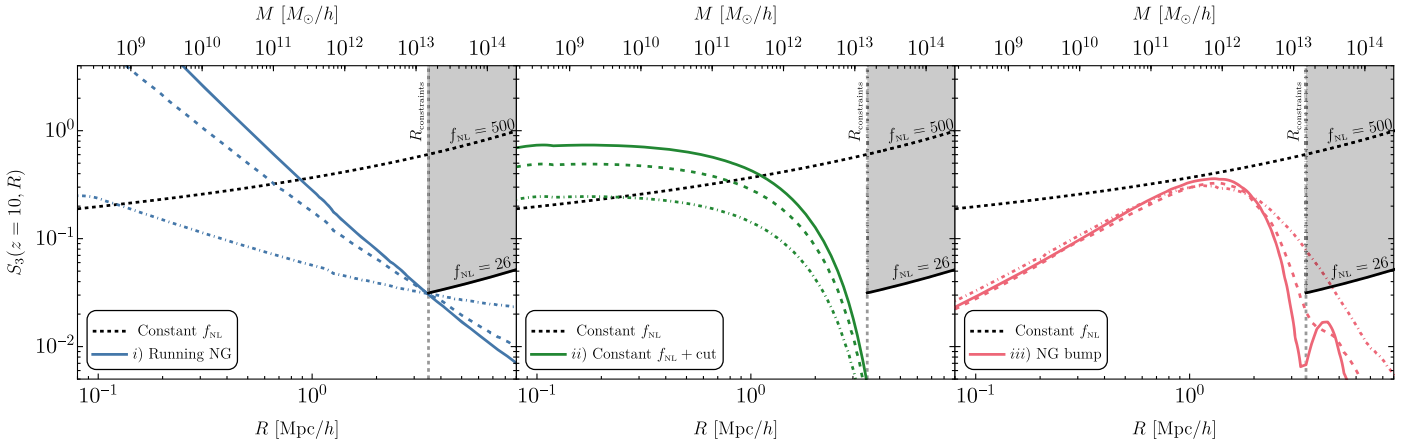


**Figure 4.** Skewness  $S_3$  as a function of scale  $R$  (or halo mass at  $z = 10$ , indicated at the top). The gray region corresponds to values of  $S_3$  obtained using excluded values of  $f_{\text{NL}}$  due to constraints from Castorina et al. (2019), assuming local-type NGs. We use a limiting value of  $f_{\text{NL}} = 26$  at the 95% confidence level using  $k_{\text{max}} = 0.3 h \text{ Mpc}^{-1}$  for a conservative assumption on the response of quasars to the NGs. We indicate  $S_3$  obtained with the various models considered in this work with the same colors used in Figure 3 as labeled in the insets.

A first case is the so-called running NG (Sefusatti et al. 2009) for which

$$\text{i) } f_{\text{NL}}(k) = f_{\text{NL}}^0 \left( \frac{k}{k_{\text{max}}} \right)^{n_{f_{\text{NL}}}}, \quad (17)$$

where, depending on the running, we consider

$$\begin{aligned} f_{\text{NL}}^0 &= 17 & \text{for } n_{f_{\text{NL}}} &= 1, \\ f_{\text{NL}}^0 &= 8.3 & \text{for } n_{f_{\text{NL}}} &= 2, \\ f_{\text{NL}}^0 &= 5.6 & \text{for } n_{f_{\text{NL}}} &= 2.4. \end{aligned} \quad (18)$$

The corresponding stellar mass densities are plotted in Figure 3 (left panel) and compared to the JWST data. We observe that a sufficiently large  $n_{f_{\text{NL}}} \gtrsim 2$  may help in reducing the tension, but it gives rise to a too-steep HMF tilted toward small halo masses that can hardly reach the largest data point at a redshift of  $z = 10$ , while being compatible with the others. In Figure 4 we plot the corresponding skewness  $S_3$ , where we have chosen  $k_{\text{max}} \simeq k_{\text{constraints}}$  to be the smallest scale constrained by large-scale structure (LSS) observations (see Sabti et al. 2021). The amplitude of  $f_{\text{NL}}(k_{\text{max}})$  has been fixed such that  $S_3$  saturates the current bound from the LSS.<sup>11</sup>

A possible solution to this problem is to take a  $f_{\text{NL}}(k)$  such that it is constant up to some scale  $k_{\text{cut}}$  (corresponding to a halo mass  $M_{\text{cut}}$ ) that vanishes at smaller momenta, such that (see, e.g., Sabti et al. 2021)

$$\begin{aligned} \text{ii) } B_{\zeta}(k_1, k_2, k_3) &= \frac{6}{5} f_{\text{NL}}^0 P_{\zeta}(k_2) P_{\zeta}(k_3) \\ &\times \left[ \prod_{i=1}^3 \Theta(k_i - k_{\text{cut}}) + \text{perm.} \right]. \end{aligned} \quad (19)$$

Such scale-dependent NGs can be obtained in inflationary models, where, besides the inflation field, there is another spectator field which experiences a transition from massless to

massive at a scale of  $\approx k_{\text{cut}}$  (Riotto & Sloth 2011). The corresponding result is shown in Figure 3 (central panel), where we plot the stellar mass density above  $M_*$  assuming different values of  $f_{\text{NL}}^0$  and the scale where the NGs are switched off corresponding to  $M_{\text{cut}} = 10^{12} M_{\odot}$ . This indicates that, in order to reach the JWST observations, large NGs are needed at least starting from masses below  $\approx 10^{12} M_{\odot}$ . The resulting shape of  $S_3$  obtained in this scenario is shown in Figure 4. Note that these large values of  $f_{\text{NL}}^0$  might be in tension with the constraints quoted by Sabti et al. (2021), which strongly depend on  $k_{\text{cut}}$ .

Finally, we consider a model in which the NG correction is localized within a bump at scales close the one observed by Labbe et al. (2022). We assume the functional form

$$\text{iii) } f_{\text{NL}}(k) = \frac{f_{\text{NL}}^0}{\sqrt{2\pi}w} \exp \left[ -\frac{\log^2(k/k_0)}{2w^2} \right] \quad (20)$$

and fix the central scale to be  $k_0 = 1.4 h \text{ Mpc}^{-1}$ , which corresponds to the masses detected by Labbe et al. (2022) at a redshift of  $z = 10$ . In Figure 3 we show the corresponding stellar mass density above  $M_*$  with varying assumptions on the width of the bump  $w$ , while the resulting skewness is plotted in Figure 4. We see that a large normalization  $f_{\text{NL}}^0$  and a relatively narrow width may allow for a reduction in the tension between the JWST observations and the cosmological model.

## 4. Conclusions

In this paper we have investigated whether changing the initial conditions of cosmological perturbations by adding some amount of NG helps in boosting the formation of massive and bright galaxies, as recently reported in the literature thanks to the new data collected by the JWST.

We tested our modeling of the NG correction of the HMF by adopting  $N$ -body simulations and checking whether the NG scenarios that are compatible with current large-scale and low-redshift observations may help explain the recent data. Our findings indicate that a large and strongly scale-dependent NG (which switches on at small scales) is needed to alleviate the tension between the cosmological model and the observations.

<sup>11</sup> Note that the model of Equation (17), besides being too steep to explain the JWST observations, produces also a very large skewness at small scales (see Figure 4). These large values would be in contrast with the truncation made on the Edgeworth expansion when neglecting the effects of the kurtosis, etc., in the calculation of the HMF.

We have modeled the halo mass distribution with the Tinker model (Tinker et al. 2010), which was used in the model validation against the  $N$ -body simulations. Notice, however, that different choices were adopted in the literature (e.g., the Sheth–Tormen mass function; Sheth & Tormen 2002) that led to larger HMF tails and, consequently, to smaller values of  $f_{\text{NL}}$  to alleviate the tension. We have verified this intuition by performing our analysis using the Sheth–Tormen mass function, for which the values of  $f_{\text{NL}}$  needed to alleviate the tension are around a factor of two smaller.

We notice once again that the small evolution of the HMF between redshifts of 8 and 10 reported in Labbe et al. (2022) poses a threat to our explanation as it is not easily captured in the models we tested and would need a rather artificial redshift dependence of the theoretical prediction. Such a caveat appears to be valid for most of the solutions recently proposed in the literature. It should be noted that our analysis does not include a complete assessment of parameter degeneracies within the  $\Lambda$ CDM model. In particular,  $\sigma_8$ , which parameterizes the amplitude of matter fluctuations, is also known to provide an enhancement on the tail of the HMF. Leaving all other cosmological parameters fixed and setting  $f_{\text{NL}} = 0$ , we have verified that explaining the observed galaxies would require values of  $\sigma_8 \gtrsim 0.9$ , which are significantly excluded by Planck (Aghanim et al. 2020).


We are aware that there are several uncertainties related to the JWST measurements, which might solve the tension with respect to the  $\Lambda$ CDM model independently from NGs. First of all, uncertainties in the calibration of JWST data may impact the redshift determinations, see, e.g., Table 4 in Adams et al. (2023). Current measurements rely on identifying high-redshift candidates using photometric template fitting which however are not tested at such high redshifts (Steinhardt et al. 2022). Another possibly large uncertainty is added in the estimation of  $M_*$ . For this, the Chabrier initial mass function is typically adopted (Chabrier 2003), which however is tested at much lower masses and redshifts. Furthermore, the effect of a large scatter in the star formation (Mirocha & Furlanetto 2023) as well as the impact of dust attenuation (Ziparo et al. 2022) may introduce further contamination in the mass estimations. Finally, if the data also include very bright lines from other sources (such as active galactic nuclei) beyond the stellar continuum, one may also get a contaminated measurement of masses (see, e.g., Endsley et al. 2022). Spectroscopic follow-up and further testing of these astrophysical uncertainties will soon shed more light on this issue.

The authors would like to thank Pierluigi Monaco for very useful comments on the draft and for discussions on the possible sources of uncertainty in the JWST measurements. M. B. acknowledges support from the NWO project ‘‘Cosmic origins from simulated universes’’ for the computing time allocated to run a subset of the EOS simulations on SNELLIUS, a supercomputer that is part of the Dutch National Computing Facilities. G.F. acknowledges financial support provided under the European Union’s H2020 ERC, Starting Grant Agreement No. DarkGRA–757480 and under the MIUR PRIN program, and support from the Amaldi Research Center funded by the MIUR program ‘‘Dipartimento di Eccellenza’’ (CUP: B81I18001170001). This work was supported by the EU Horizon 2020 Research and Innovation Programme under the Marie Skłodowska-Curie Grant Agreement No.

101007855. A.R. acknowledges financial support provided by the Boninchi Foundation.

## ORCID iDs

Matteo Biagetti  <https://orcid.org/0000-0002-5097-479X>

Gabriele Franciolini  <https://orcid.org/0000-0002-6892-9145>

## References

- Achitouv, I., Wagner, C., Weller, J., & Rasera, Y. 2014, *JCAP*, 2014, 077
- Achitouv, I. E., & Corasaniti, P. S. 2012, *JCAP*, 2012, 002
- Adams, N. J., Conselice, C. J., Ferreira, L., et al. 2023, *MNRAS*, 518, 4755
- Aghanim, N., Akrami, Y., Ashdown, M., et al. 2020, *A&A*, 641, A6
- Agullo, I., & Shandera, S. 2012, *JCAP*, 2012, 007
- Akrami, Y., Arroja, F., Ashdown, M., et al. 2020, *A&A*, 641, A9
- Atek, H., Shuntov, M., Furtak, L. J., et al. 2023, *MNRAS*, 519, 1201
- Bartolo, N., Komatsu, E., Matarrese, S., & Riotta, A. 2004, *PhR*, 402, 103
- Becker, A., Huterer, D., & Kadota, K. 2011, *JCAP*, 2011, 006
- Becker, A., Huterer, D., & Kadota, K. 2012, *JCAP*, 2012, 034
- Behroozi, P. S., Wechsler, R. H., & Wu, H.-Y. 2013, *ApJ*, 762, 109
- Biagetti, M. 2019, *Galax*, 7, 71
- Biagetti, M., Desjacques, V., & Riotta, A. 2013a, *MNRAS*, 429, 1774
- Biagetti, M., Lazeyras, T., Baldauf, T., Desjacques, V., & Schmidt, F. 2017, *MNRAS*, 468, 3277
- Biagetti, M., Perrier, H., Riotta, A., & Desjacques, V. 2013b, *PhRvD*, 87, 063521
- Blas, D., Lesgourgues, J., & Tram, T. 2011, *JCAP*, 2011, 034
- Borgani, S., Coles, P., Moscardini, L., & Plionis, M. 1994, *MNRAS*, 266, 524
- Byrnes, C. T., Enqvist, K., Nurmi, S., & Takahashi, T. 2011, *JCAP*, 2011, 011
- Byrnes, C. T., Gerstenlauer, M., Nurmi, S., Tasinato, G., & Wands, D. 2010, *JCAP*, 2010, 004
- Castorina, E., Hand, N., Seljak, U., et al. 2019, *JCAP*, 2019, 010
- Chabrier, G. 2003, *PASP*, 115, 763
- Chen, X. 2005, *PhRvD*, 72, 123518
- Chongchitnan, S., & Silk, J. 2010, *ApJ*, 724, 285
- Cohn, J. D., & White, M. 2008, *MNRAS*, 385, 2025
- Dalal, N., Doré, O., Huterer, D., & Shirokov, A. 2008, *PhRvD*, 77, 123514
- Desjacques, V., & Seljak, U. 2010, *PhRvD*, 81, 023006
- Despali, G., Giocoli, C., Angulo, R. E., et al. 2015, *MNRAS*, 456, 2486
- Endsley, R., Stark, D. P., Whittler, L., et al. 2022, arXiv:2208.14999
- Evrard, A. E., MacFarland, T. J., Couchman, H. M. P., et al. 2002, *ApJ*, 573, 7
- Finkelstein, S. L., Bagley, M. B., Arrabal Haro, P., et al. 2022, *ApJL*, 940, L55
- Giannantonio, T., Porciani, C., Carron, J., Amara, A., & Pillepich, A. 2012, *MNRAS*, 422, 2854
- Gong, Y., Yue, B., Cao, Y., & Chen, X. 2022, arXiv:2209.13757
- Gooding, A. K., Park, C., Spergel, D. N., Turok, N., & Gott, R. I. 1992, *ApJ*, 393, 42
- Harikane, Y., Ouchi, M., Oguri, M., et al. 2022, arXiv:2208.01612
- Huang, Q.-G. 2010a, *JCAP*, 2010, 026
- Huang, Q.-G. 2010b, *JCAP*, 2010, 017
- Jenkins, A., Frenk, C. S., White, S. D. M., et al. 2001, *MNRAS*, 321, 372
- Khoury, J., & Piazza, F. 2009, *JCAP*, 2009, 026
- Labbe, I., van Dokkum, P., Nelson, E., et al. 2022, arXiv:2207.12446
- Liu, B., & Bromm, V. 2022, *ApJL*, 937, L30
- Lovell, C. C., Harrison, I., Harikane, Y., Tacchella, S., & Wilkins, S. M. 2023, *MNRAS*, 518, 2511
- LoVerde, M., Miller, A., Shandera, S., & Verde, L. 2008, *JCAP*, 2008, 014
- Lukic, Z., Heitmann, K., Habib, S., Bashinsky, S., & Ricker, P. M. 2007, *ApJ*, 671, 1160
- Matarrese, S., Lucchin, F., Messina, A., & Moscardini, L. 1991, *MNRAS*, 253, 35
- Matarrese, S., Verde, L., & Jimenez, R. 2000, *ApJ*, 541, 10
- Menci, N., Castellano, M., Santini, P., et al. 2022, *ApJL*, 938, L5
- Mirocha, J., & Furlanetto, S. R. 2023, *MNRAS*, 519, 843
- Moscardini, L., Matarrese, S., Lucchin, F., & Messina, A. 1991, *MNRAS*, 248, 424
- Naidu, R. P., Oesch, P. A., Setton, D. J., et al. 2022, arXiv:2208.02794
- Park, C., Spergel, D. N., & Turok, N. 1991, *ApJL*, 372, L53
- Pillepich, A., Porciani, C., & Hahn, O. 2010, *MNRAS*, 402, 191
- Reed, D., Gardner, J., Quinn, T., et al. 2003, *MNRAS*, 346, 565
- Reed, D. S., Bower, R., Frenk, C. S., Jenkins, A., & Theuns, T. 2007, *MNRAS*, 374, 2
- Riotta, A., & Sloth, M. S. 2011, *PhRvD*, 83, 041301

- Sabti, N., Muñoz, J. B., & Blas, D. 2021, [JCAP](#), **2021**, 010
- Scoccimarro, R. 1998, [MNRAS](#), **299**, 1097
- Scoccimarro, R., Hui, L., Manera, M., & Chan, K. C. 2012, [PhRvD](#), **85**, 083002
- Sefusatti, E., Liguori, M., Yadav, A. P. S., Jackson, M. G., & Pajer, E. 2009, [JCAP](#), **2009**, 022
- Sheth, R. K., & Tormen, G. 2002, [MNRAS](#), **329**, 61
- Springel, V. 2005, [MNRAS](#), **364**, 1105
- Stahl, C., Montandon, T., Famaey, B., Hahn, O., & Ibata, R. 2023, [JCAP](#), **2023**, 024
- Steinhardt, C. L., Kokorev, V., Rusakov, V., Garcia, E., & Sneppen, A. 2022, [arXiv:2208.07879](#)
- Tinker, J., Kravtsov, A. V., Klypin, A., et al. 2008, [ApJ](#), **688**, 709
- Tinker, J. L., Robertson, B. E., Kravtsov, A. V., et al. 2010, [ApJ](#), **724**, 878
- Warren, M. S., Abazajian, K., Holz, D. E., & Teodoro, L. 2006, [ApJ](#), **646**, 881
- Weinberg, D. H., & Cole, S. 1992, [MNRAS](#), **259**, 652
- Yan, H., Ma, Z., Ling, C., et al. 2022, [ApJL](#), **942**, L9
- Ziparo, F., Ferrara, A., Sommovigo, L., & Kohandel, M. 2022, [arXiv:2209.06840](#)